

Calculations of Oxygen Adsorption-Induced Surface Reconstruction and Oxide Formation on Cu(100)

Xin Lian,^{†,§} Penghao Xiao,^{‡,§} Renlong Liu,^{*,†} and Graeme Henkelman^{*,‡}

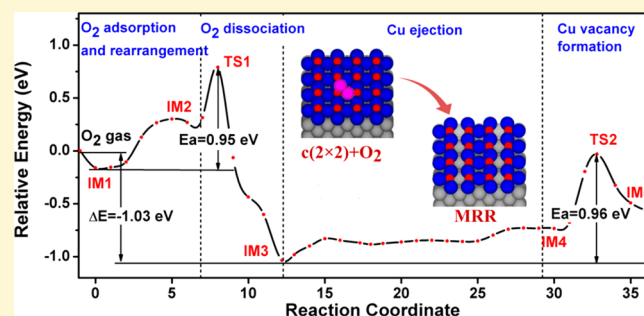
[†]College of Chemistry and Chemical Engineering, Chongqing University, Chongqing 400030, China

[‡]Department of Chemistry and the Institute for Computational and Engineering Sciences, University of Texas at Austin, Austin, Texas 78712-0165, United States

S Supporting Information

ABSTRACT: The energetics and kinetics of the missing-row reconstruction (MRR) and missing-row island formation on the Cu(100) surface are investigated using density functional theory calculations. We find that copper ejection from the $c(2 \times 2)$ surface is made energetically possible by the presence of surface-adsorbed O_2 molecules. The barrier for MRR formation via this ejection mechanism is calculated to be 0.96 eV, consistent with the experimentally observed formation temperature of 400 K. The reaction pathways between Cu and O_2 result in the formation of Cu–O chains on the $c(2 \times 2)$ surface, which can grow from the –O–Cu–O– trimer at least up to the –Cu–O–Cu–O–Cu– pentamer.

Remarkably, these chains can both diffuse rapidly and change their orientation on the surface, allowing them to assemble into longer Cu–O chains. Facile diffusion of the Cu–O chains occurs via a collective mechanism which limits the number of broken Cu–O bonds. Perpendicular to the Cu–O rows, the chains hop first at one end and then the other. Parallel, the chains move as an inchworm does, again, one end advancing before the other. When two Cu–O chains become parallel neighbors, they are able to pull additional Cu atoms from the $c(2 \times 2)$ subsurface with a barrier of 0.65 eV, forming an MRR island with the MRR structure both in the surface and subsurface layers. The set of oxidation and diffusion mechanisms calculated here provide a detailed picture of MRR and MRR island formation on the Cu(100) surface.



1. INTRODUCTION

Upon exposure to an oxygen atmosphere, metal surfaces typically undergo a series of phase transitions starting from oxygen chemisorption, to oxygen-induced surface reconstruction, to bulk oxide formation. The interaction between oxygen and a metal surface has received much attention due to its critical role in many important applications^{1–7} such as heterogeneous catalysis, surface passivation, and thin-film processing. It has recently been shown that the catalytic performance of some oxides is better than that of their pure metal counterparts.^{3,8} These applications provide motivation for a fundamental study of how metal surfaces respond to adsorbed oxygen at different coverages and the mechanism governing surface oxide layer formation.

Oxygen chemisorption on the Cu(100) surface, as a model system, has been extensively studied. On the basis of investigations using X-ray photoelectron spectroscopy (XPS) and scanning tunneling microscopy (STM), the oxidation of the Cu(100) surface proceeds in three distinct steps:^{9,10} (1) dissociative adsorption of O_2 , the formation of the Cu- $c(2 \times 2)$ phase, and the Cu- $(2\sqrt{2} \times \sqrt{2})R45^\circ$ -O missing-row reconstruction (MRR) at an oxygen coverage of 0.5 monolayers (MLs); (2) the growth of well-ordered protruding missing-row

islands; and (3) the nucleation of Cu_2O islands with oxygen in the subsurface.

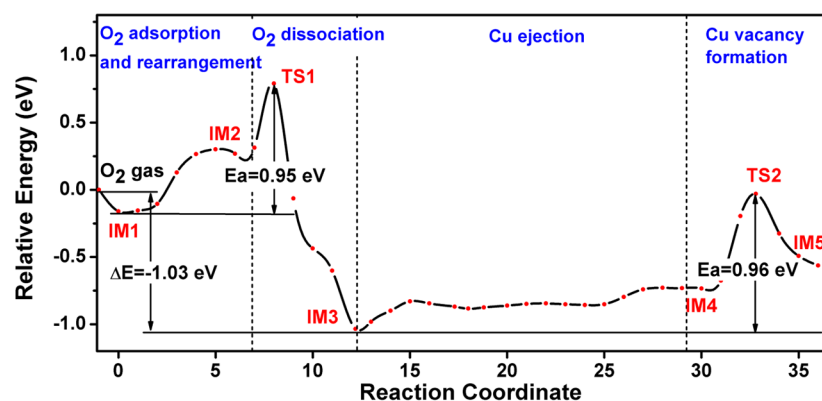
Step 1, which has been widely studied using experimental and computational techniques, is of particular interest.^{11–24} Early reports showed that the $c(2 \times 2)$ phase evolves into the MRR structure at oxygen coverages around 0.5 monolayers (ML).^{11,12,20,25–27} Using STM,¹⁶ Jensen et al. inferred that the MRR is formed through the ejection of Cu from every fourth row of the $c(2 \times 2)$ surface. This mechanism by which the MRR is initiated from $c(2 \times 2)$ domains was supported by subsequent experimental studies.^{15,18,22} Theoretical studies have also explored the mechanism of transition from $c(2 \times 2)$ to MRR at the atomic scale. Using density functional theory (DFT) calculations, Lee et al.²⁸ proposed a Cu ejection and diffusion path with a barrier as high as 2 eV. Kangas et al.²⁹ suggested another mechanism in which Cu adatoms are introduced on the $c(2 \times 2)$ surface, lowering the barrier for Cu ejection to 0.54 eV.

In comparison with the MRR formation (step 1), there are far fewer studies to address the subsequent changes in surface

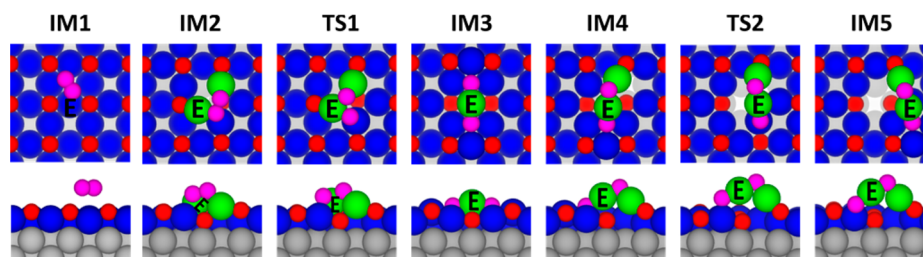
Received: July 4, 2016

Revised: January 26, 2017

Published: January 27, 2017



(a)



(b)

Figure 1. (a) MEP plot for Cu atom ejection in the presence of an O_2 molecule on the Cu(100)- $c(2 \times 2)$ surface. (b) Upper panels are top views, and the lower panels are side views of the key intermediate (IM) and transition states (TS). For illustration purposes, the top-layer Cu and O atoms are depicted as blue and red spheres, and the substrate Cu atoms are gray; adsorbed O and prominent Cu atoms are magenta and green, respectively. The ejected Cu is labeled with an E.

morphology (steps 2 and 3).^{30–33} Using XPS and STM,⁹ Lampimaki et al. identified well-ordered missing-row islands which are 1.8 Å higher than the surrounding substrate. They attributed the formation of these islands to the release of surface Cu atoms during the MRR formation. Lahtonen et al.¹⁰ found that the interface between the islands and substrate plays a key role in the subsequent oxidation and the growth of Cu_2O islands. Kangas et al. and Lee et al. used DFT calculations^{34–36} to demonstrate that the concentration of subsurface oxygen is the key to oxide formation.

Despite numerous studies, there is still a lack of fundamental understanding of the crossover between oxygen chemisorption and subsequent surface reconstruction(s). Although Lee and Kangas proposed two different mechanisms by which Cu atoms are pulled from the substrate to form a surface oxide, we do not expect either to be facile under typical experimental conditions. The Lee mechanism²⁸ has a barrier of 2 eV and will therefore not proceed at 400 K when oxidation is observed experimentally.^{9,10} The Kangas mechanism²⁹ is also unlikely because it requires the presence of Cu adatoms, which are energetically unfavorable on the surface and would be saturated with oxygen under oxidizing conditions.

In this paper, we present a different Cu ejection mechanism which is active in the presence of O_2 on the $c(2 \times 2)$ surface. In particular, we discuss how the ejected Cu atoms diffuse, accompanied by O atoms, to form well-ordered missing-row islands; a topic that is largely unexplored.

2. COMPUTATIONAL METHOD

DFT calculations were performed using the Vienna Ab-initio Simulation Package^{37–39} with the PBE^{40,41} generalized gradient

approximation functional. The projector augmented wave method was used to describe the core electrons. Valence electrons were described by a plane wave basis with a cutoff energy of 350 eV.^{42,43} The Brillouin-zone integration was performed using a $(2 \times 2 \times 1)$ Monkhorst–Pack K-point mesh.⁴⁴ The surface was modeled by a periodic slab consisting of four Cu layers. The bottom layer was held fixed in bulk positions, while atoms in the other layers were relaxed until their residual forces were less than 0.01 eV/Å. Periodic slabs along the z-direction were separated by a vacuum region of 15 Å. All of our calculations were spin-averaged except for those involving free molecular O_2 , which was spin polarized. Adsorption was done on one side of the slab only. In consideration of the fact that long-range dispersion interactions will play a role in O_2 adsorption and dissociation on the Cu- $c(2 \times 2)$ surface, the DFT-D3 method of Grimme⁴⁵ was employed to include dispersion interactions within the PBE calculations. We used the climbing image nudged elastic band method⁴⁶ to determine diffusion pathways and energy barriers.

The rate constant for each reaction was determined from the energy barrier according to the harmonic transition state theory:

$$k = A e^{-E_a/k_B T} \quad (1)$$

where A is the prefactor accounting for entropic contributions, E_a is the activation energy, k_B is the Boltzmann constant, and T is the temperature. For simplicity, all prefactors are taken as 10^{13} /s.

3. RESULTS

3.1. Cu Atom Ejection (MRR Nucleation). The minimum energy path (MEP) for the surface Cu ejection in the presence of an adsorbed O_2 molecule on the $c(2 \times 2)$ surface is shown in Figures 1a and b. The reaction can be divided into four stages: O_2 adsorption and rearrangement, O_2 dissociation, Cu atom ejection and association to surface O atoms, and finally Cu vacancy formation. In the first step, the O_2 molecule adsorbs on

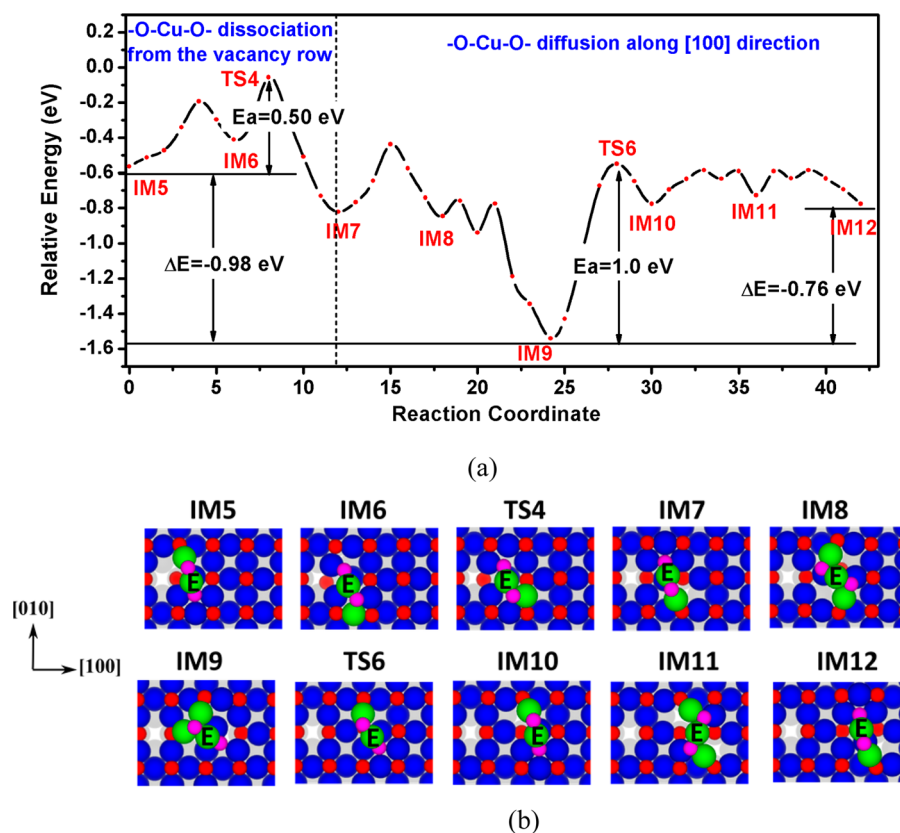


Figure 2. (a) MEP plot for $-\text{O}-\text{Cu}-\text{O}$ trimer diffusion along the $[100]$ direction on the $\text{Cu}(100)-c(2 \times 2)$ surface with (b) intermediate and transition states. The color scheme is as in Figure 1.

the $c(2 \times 2)$ surface to form the IM1. The adsorption energy is -0.16 eV, including dispersion interactions calculated with the DFT-D3 method. Then, two Cu atoms in IM1 rise slightly out of the surface (IM2) with a barrier of 0.45 eV. Next, O_2 dissociates into two O atoms, and they combine with a Cu atom (IM3) to form a stable $-\text{O}-\text{Cu}-\text{O}-$ trimer with a barrier of 0.52 eV. The O_2 dissociation results in a significant energy drop of 1.03 eV with respect to O_2 in the gas phase. After O_2 dissociation, the inclusion of van der Waals interactions results in only a minor change in the energetics and is not considered in the following calculations. In the third step, the O atoms pull two Cu atoms out of the surface with a barrier of 0.3 eV to form a short $-\text{Cu}-\text{O}-$ chain (IM4) lying ~ 2.0 Å higher than the $c(2 \times 2)$ surface. Finally, one end (the lower magenta O in the top view of Figure 1b) of the raised $-\text{Cu}-\text{O}-$ chain swings to an adjacent hollow site, forming a Cu vacancy. The energy barrier for this step is 0.68 eV, and the final state (IM5) is 0.16 eV higher than IM4. The highest barrier in the Cu ejection process is 0.96 eV, produced by the transit from IM3 to IM5. From O_2 in the gas phase to the formation of the Cu vacancy on the $c(2 \times 2)$ surface, the energy released is 0.56 eV.

In our mechanism, the Cu ejection barrier is reduced to less than 1.0 eV in the presence of an O_2 molecule. The low barrier indicates that this reaction can readily proceed at the temperature when $\text{Cu}(100)$ oxidation is observed experimentally (373 – 500 K). The energy decrease along the reaction path implies that the transition is thermodynamically favorable.

3.2. Cu–O Units Growth and Diffusion. Once a Cu atom is ejected from the surface, a natural question to ask is if the Cu–O units are mobile and if the Cu–O chain will grow longer

before it diffuses away from the vacancy site. To answer these questions, we investigate possible Cu–O growth and diffusion mechanisms in the following sections.

3.2.1. $-\text{O}-\text{Cu}-\text{O}-$ Trimer Diffusion. There are two possible directions for the $-\text{O}-\text{Cu}-\text{O}-$ trimer to diffuse on the $c(2 \times 2)$ surface. One is along the $[100]$ direction, as shown in Figures 2a and b; the other is along the $[010]$ direction, as shown in Figures 3a and b. The side views of these two diffusion paths are shown in Figures S1 and S2 (Supporting Information).

Starting from IM5 in Figure 2b, two steps are involved in the diffusion of the $-\text{O}-\text{Cu}-\text{O}-$ trimer along the $[100]$ direction. The first step is that the $-\text{O}-\text{Cu}-\text{O}-$ trimer leaves the Cu vacancy or preexisting row (column in the figure). The second is that the $-\text{O}-\text{Cu}-\text{O}-$ trimer diffuses on the $c(2 \times 2)$ surface away from the Cu vacancy. From IM5 to IM7, the Cu vacancy is separated from the ejected Cu, nucleating an MRR unit. From IM7 to IM10, the upper magenta O leaves the hollow site to attach on the top of the Cu atom in the right neighbor, pulling it out of the surface. Simultaneously, the lower magenta O falls into the hollow site on the right, and the connected Cu atom drops back into the surface. The intermediate IM9 contains a stable tetrahedral structure composed of one O atom and three Cu atoms. Escaping from IM9 to IM10 requires a high barrier of 1.0 eV. The subsequent diffusion starting from IM10 to the end of the path is facile with barriers less than 0.2 eV. From IM7 to IM12, the $-\text{O}-\text{Cu}-\text{O}-$ trimer moves one $[100]$ - (1×2) lattice spacing on the $c(2 \times 2)$ surface.

The MEP plot and intermediate images of the $-\text{O}-\text{Cu}-\text{O}-$ trimer diffusing along the $[010]$ direction are shown in Figures 3a and b, respectively. Once a vacancy is formed, the trimer

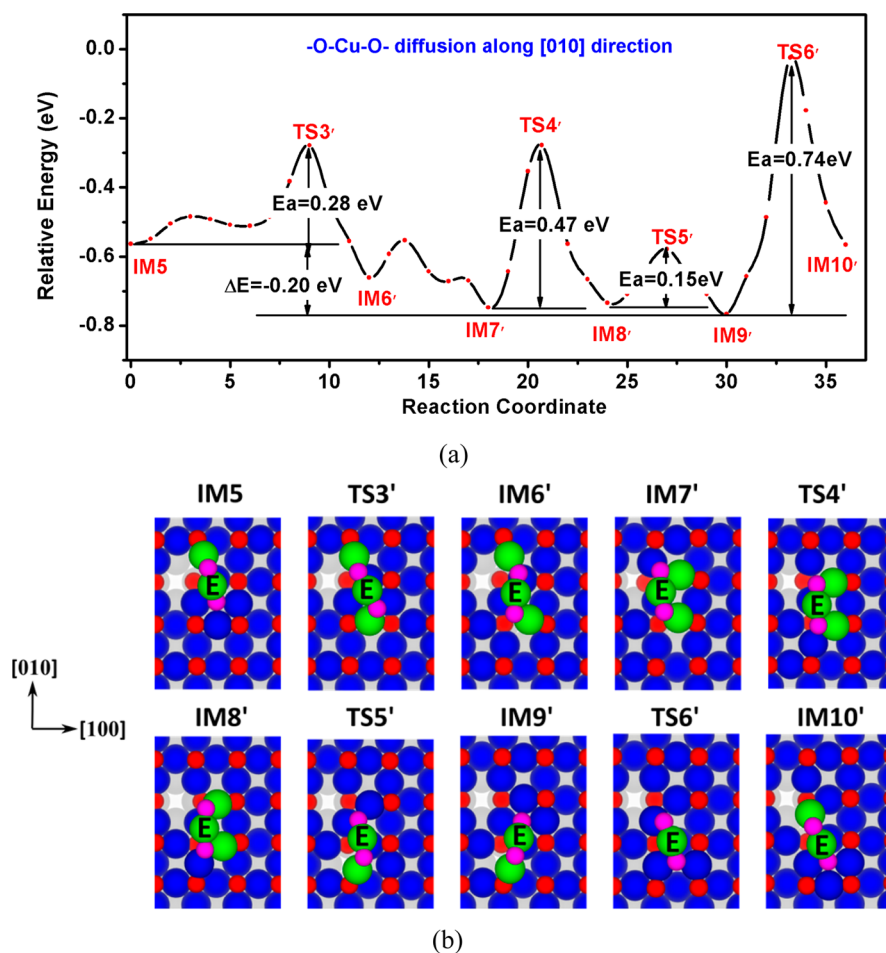


Figure 3. (a) MEP plot for the $-O-Cu-O$ trimer diffusing along the $[010]$ direction on the $Cu(100)-c(2 \times 2)$ surface with (b) figures of intermediate and transition states.

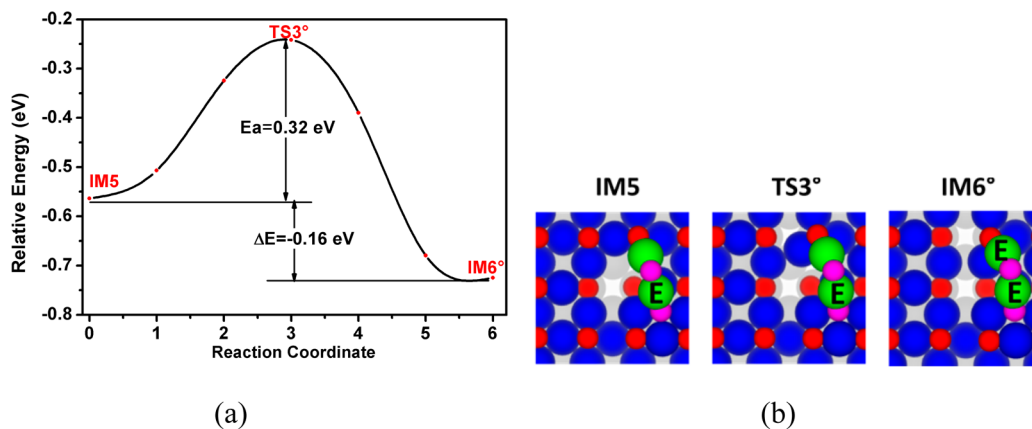


Figure 4. (a) The MEP plot for the $-Cu-O-Cu-O-$ tetramer chain formation on the $Cu(100)-c(2 \times 2)$ surface with (b) figures of intermediate and transition states.

can diffuse along the vacancy row. In the process, the terminal O either connects to a hollow site on the surface or pulls another Cu atom out of the surface to form a bridge configuration. The highest barrier for this process is 0.74 eV, which is slightly lower than that of the trimer diffusion along the $[100]$ direction, owing to the absence of trap states such as IM9 in Figure 2b.

3.2.2. $-Cu-O-Cu-O-$ Tetramer Formation and Diffusion. In the trimer structure, two O atoms are bound to one

ejected Cu atom. While the trimer can diffuse, it can also facilitate the ejection of one more Cu atoms from the surface. In order to make a $-Cu-O-Cu-O-$ tetramer chain, an adjacent Cu atom diffuses to fully eject the second Cu atom (shown as green in Figure 4b). The reaction barrier to form the tetramer structure is 0.32 eV, as shown in Figure 4a, leaving two vacancies along the missing column (IM6°) and decreasing the system energy by 0.16 eV.

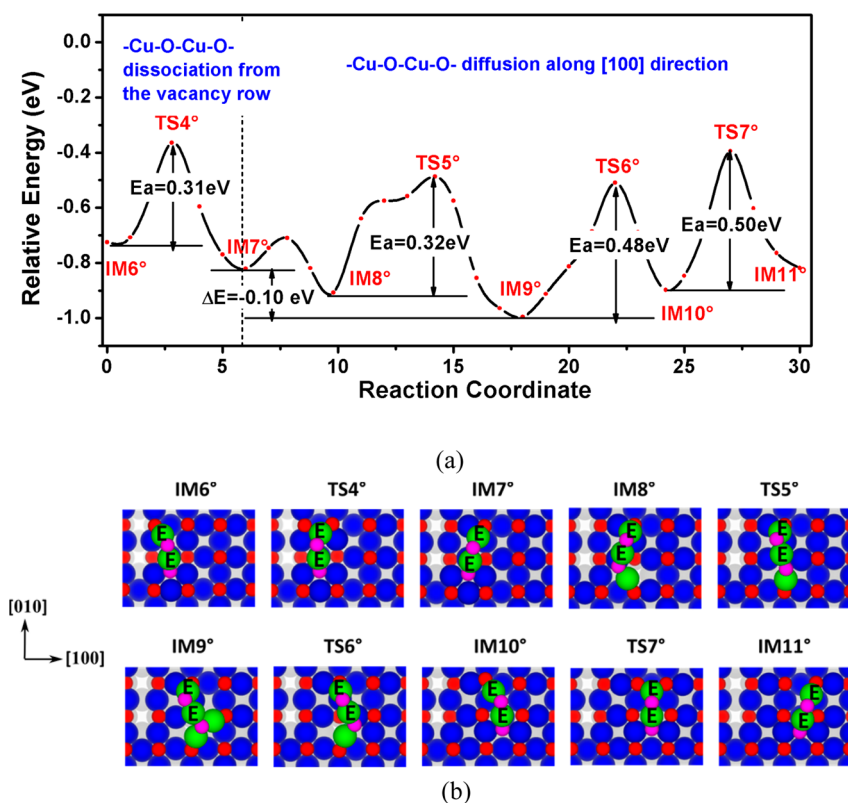


Figure 5. (a) MEP plot for $-\text{Cu}-\text{O}-\text{Cu}-\text{O}$ tetramer diffusion along the $[100]$ direction on the $\text{Cu}(100)-c(2 \times 2)$ surface with (b) intermediate and transition states.

The $-\text{Cu}-\text{O}-\text{Cu}-\text{O}-$ tetramer is able to diffuse along both Cartesian directions of the $c(2 \times 2)$ surface. Figures 5a and b show the diffusion along the $[100]$ direction, and Figures 6a and b show the diffusion along the $[010]$ direction. The side views of these two diffusion paths are shown in Figures S3 and S4.

In Figures 5a and b, similar to the trimer diffusion, the $-\text{Cu}-\text{O}-\text{Cu}-\text{O}-$ tetramer diffuses along the $[100]$ direction in two steps. From IM6° to IM7° , the tetramer diffuses away from the vacancies with a barrier of 0.31 eV. From the IM7° to IM11° , the $-\text{Cu}-\text{O}-\text{Cu}-\text{O}-$ tetramer completes a diffusion step on the $c(2 \times 2)$ surface. The top terminal Cu moves to the adjacent column, attaching to another O in the surface. The bottom terminal O then moves to the adjacent hollow site. The diffusion barrier is 0.50 eV.

Figures 6a and b depict the energy landscape of the $-\text{Cu}-\text{O}-\text{Cu}-\text{O}-$ tetramer diffusion along the $[010]$ direction. In this path, the tetramer diffuses alongside the vacancies. The terminal Cu moves along the $[010]$ direction to the adjacent row and attaches with the O atom in the surface next to a vacancy. The terminal O moves down to the adjacent hollow site as well. The highest barrier is calculated as 0.65 eV, corresponding to breaking one Cu–O bond (TSS^*).

3.2.3. $-\text{Cu}-\text{O}-\text{Cu}-\text{O}-\text{Cu}-$ Pentamer Formation and Diffusion. Similar to the formation of the $-\text{Cu}-\text{O}-\text{Cu}-\text{O}-$ tetramer, one more Cu can be pulled out from IM6° to form the $-\text{Cu}-\text{O}-\text{Cu}-\text{O}-\text{Cu}-$ pentamer. At this point, two O atoms from the O_2 dissociation are maximally coordinated to three Cu atoms. To form the pentamer, the bottom Cu atom in the vacancy row pushes up one adjacent Cu atom in the surface to form the raised $-\text{Cu}-\text{O}-\text{Cu}-\text{O}-\text{Cu}-$ pentamer, as shown in Figure 7. This process requires an energy barrier of 0.51 eV

(TS4^\wedge), resulting in three vacancies in the missing column (IM7^\wedge).

The diffusion paths for the pentamer on the $c(2 \times 2)$ surface along the $[100]$ and $[010]$ directions are shown in Figures 8 and 9, respectively. The side views of these two diffusion paths can be found in Figures S5 and S6. In Figure 8, one of terminal Cu atoms in the pentamer (IM7^\wedge) first diffuses away from the vacancies with a barrier (TSS^\wedge) of 0.36 eV. The other terminal Cu atom then follows in a similar way with a barrier of 0.37 eV. From IM9^\wedge to IM12^\wedge , the $-\text{Cu}-\text{O}-\text{Cu}-\text{O}-\text{Cu}-$ pentamer is essentially separated from the vacancy row and diffuses on the perfect $c(2 \times 2)$ surface. One terminal Cu atom moves one $[100]$ - (1×2) lattice spacing to connect to the next column O atom in the substrate, and then the other terminal Cu atom moves sequentially to attach to another O located in the same column as the first. The pentamer diffusion mechanism is reminiscent of a line segment walking along the surface with two legs. The overall diffusion barrier of this walking mechanism (TS8^\wedge) is 0.43 eV.

The process for pentamer diffusion along the $[010]$ direction is simple (Figures 9a and b). Continuing from IM8^\wedge in Figure 8b, where two terminal Cu atoms of the pentamer connect two O atoms in the substrate diagonally spanning two square units of O, the top terminal Cu atom detaches and moves one O site down with a barrier of 0.51 eV. Now the pentamer spans one square unit of O, as shown in Figure 9b (IM9^+). The other terminal Cu atom moves in the same way to connect the adjacent O atom down in the $[010]$ direction (IM10^+) with a barrier of 0.74 eV. We also considered a diffusion path starting from IM7^\wedge in Figure 8b, where both terminal Cu atoms in the pentamer always connect to two O atoms in the same column. The barrier for this path, however, is higher at 0.86 eV.

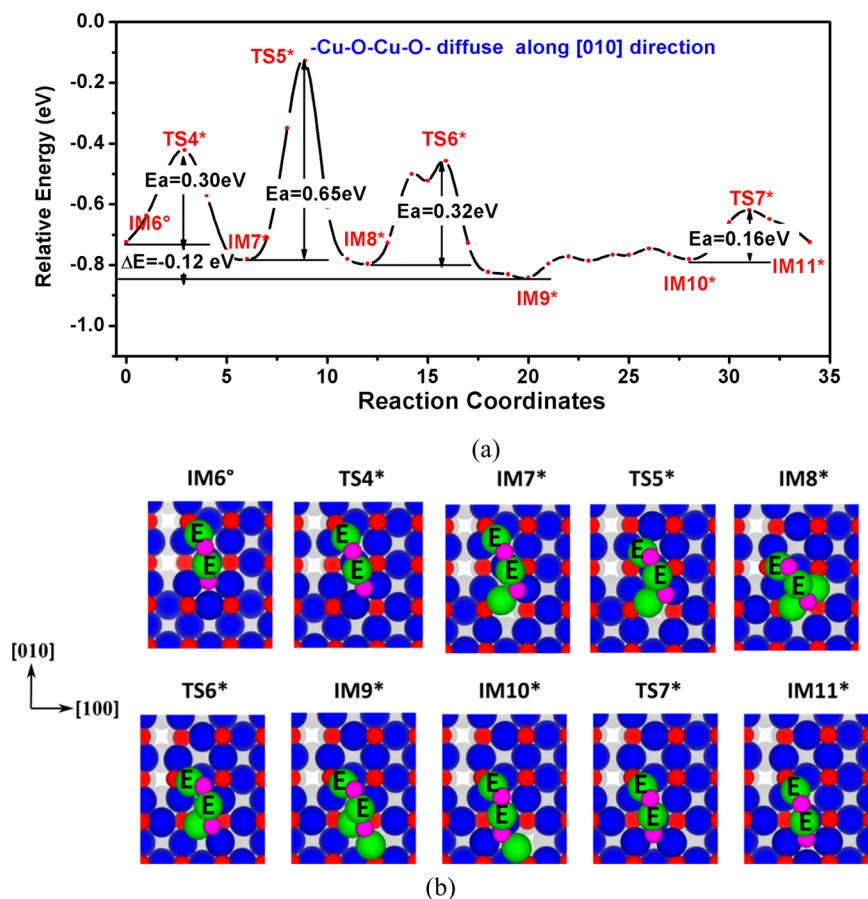


Figure 6. (a) MEP plot for $-\text{Cu}-\text{O}-\text{Cu}-\text{O}$ tetramer diffusion along the $[010]$ direction on the $\text{Cu}(100)-c(2 \times 2)$ surface with (b) figures of intermediate and transition states.

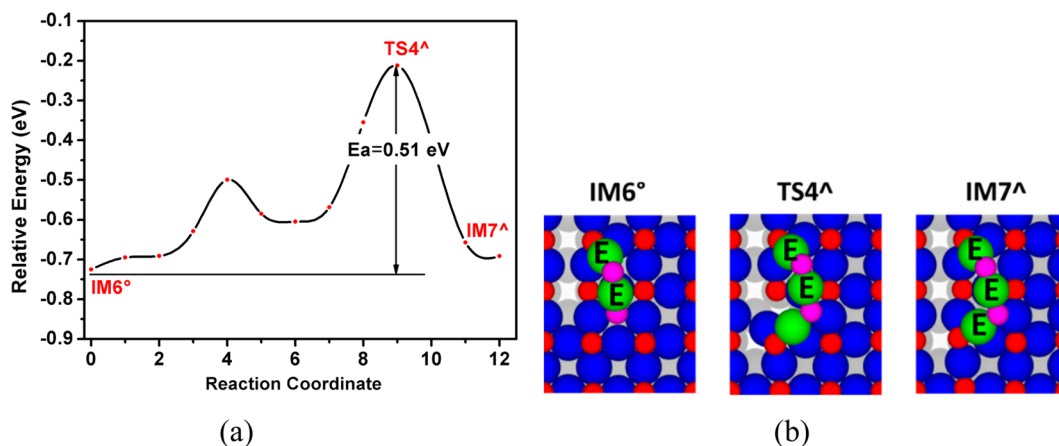


Figure 7. (a) MEP plot for $-\text{Cu}-\text{O}-\text{Cu}-\text{O}-\text{Cu}-$ pentamer chain formation on the $\text{Cu}(100)-c(2 \times 2)$ surface with (b) figures of intermediate and transition states.

The rate-limiting steps for missing-row nucleation and $-\text{Cu}-\text{O}-$ diffusion are summarized in Figure 10. The largest barrier among all the atomic processes involved in the transition between $c(2 \times 2)$ and the MRR is 1.0 eV. Once Cu atoms are ejected from the substrate, the $c(2 \times 2)$ surface operates as diffusion channels for $-\text{Cu}-\text{O}-$ chains. In our model, there are three species and six possible pathways for the $-\text{Cu}-\text{O}-$ chains to diffuse on the $c(2 \times 2)$ surface. Two general trends can be seen in this data: (i) chains of all

lengths diffuse more easily perpendicular to rather than parallel to their orientation and (ii) longer chains are more stable.

Although there may be other potential pathways unexplored here, the low energy barriers for missing-row formation in our mechanism indicate that these pathways are feasible at 400 K where the MRR is seen to form experimentally.

3.3. Cu-O Rotation. In the diffusion paths mentioned above, the $\text{Cu}-\text{O}$ chains are always parallel to the vacancy rows. A new question is considered here: can the $\text{Cu}-\text{O}$ units change their orientation and grow perpendicular to the vacancy

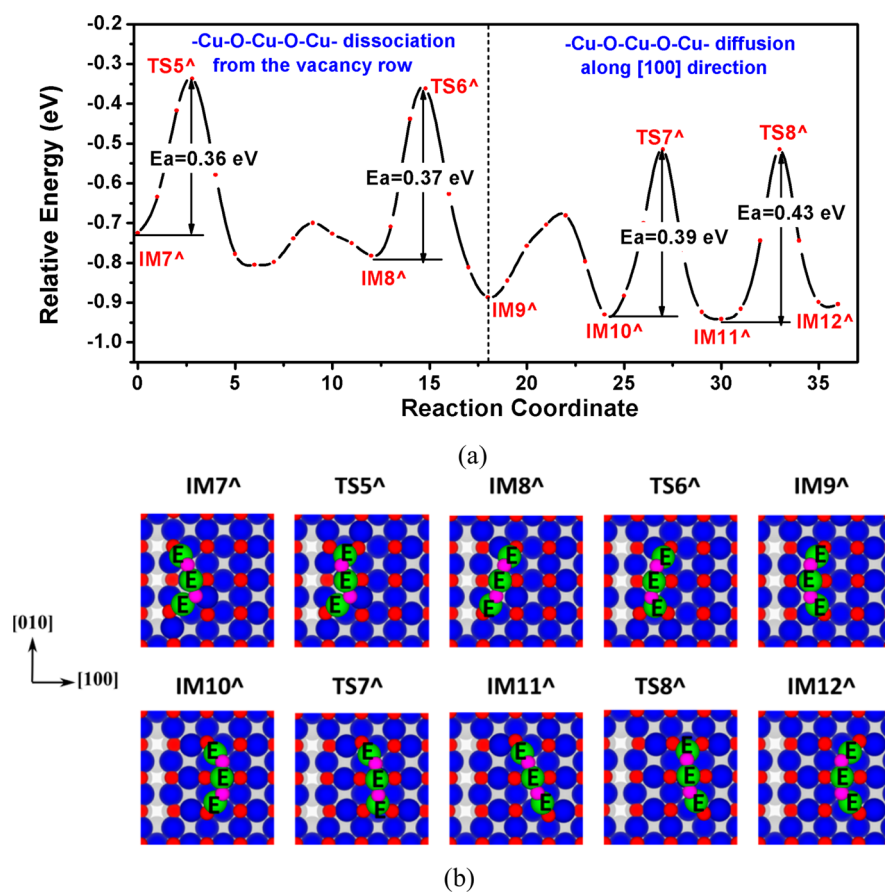


Figure 8. (a) MEP plot for $-\text{Cu}-\text{O}-\text{Cu}-\text{O}-\text{Cu}-$ pentamer diffusing along the $[100]$ direction on the $c(2 \times 2)$ surface with (b) figures of intermediate and transition states.

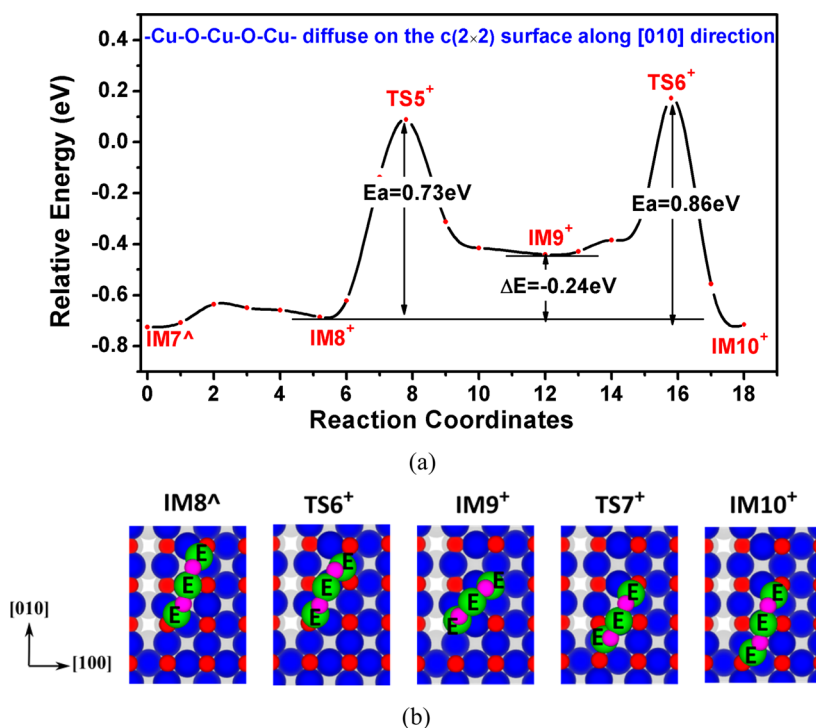


Figure 9. (a) MEP plot for $-\text{Cu}-\text{O}-\text{Cu}-\text{O}-\text{Cu}-$ pentamer diffuse along the $[010]$ direction on the $\text{Cu}(100)-c(2 \times 2)$ surface with (b) figures of intermediate and transition states.

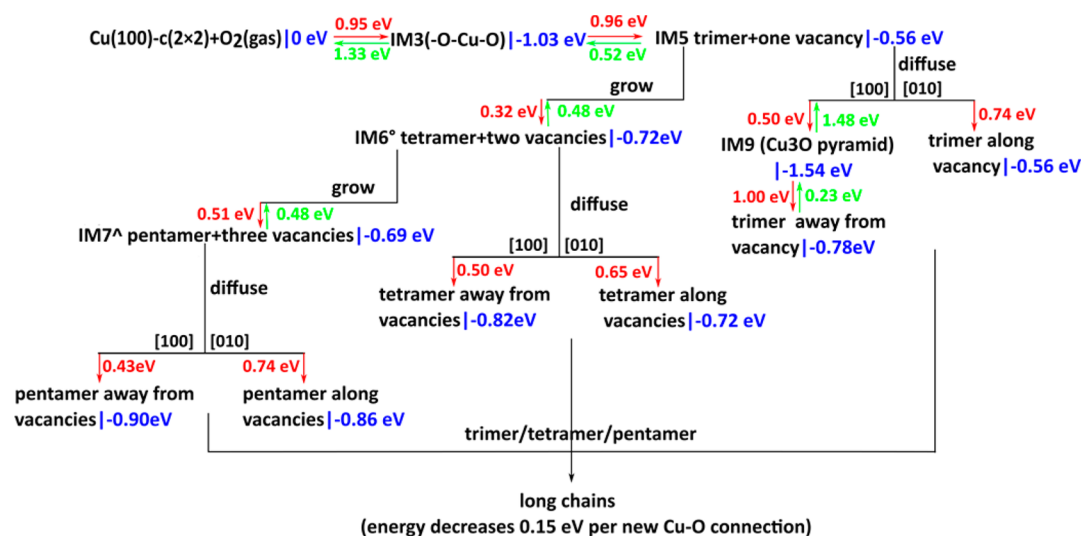


Figure 10. Schematic of missing-row nucleation and $-\text{Cu}-\text{O}-$ chain diffusion on the $\text{Cu}(100)-c(2 \times 2)$ surface. The red and green energy barriers indicate the forward and backward rate-limiting steps in each process, respectively. The blue values indicate relative energies with respect to the O_2 in the gas state.

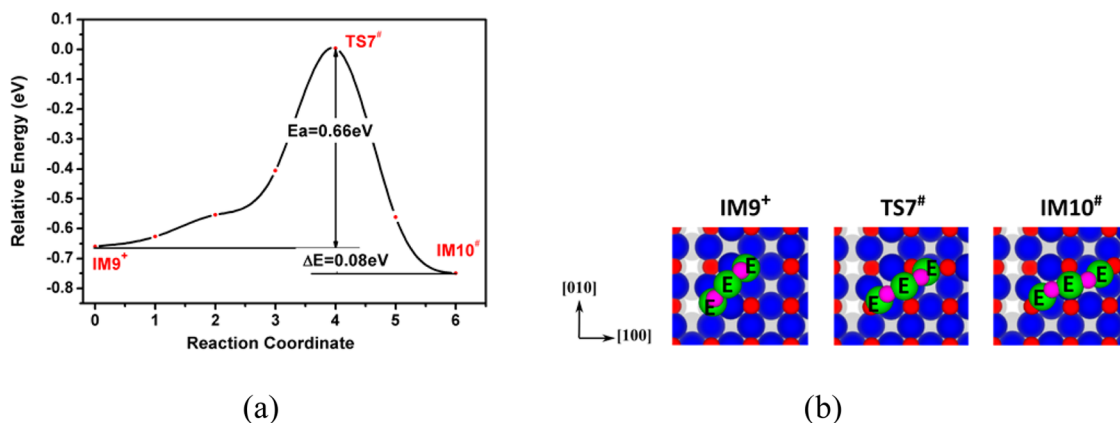


Figure 11. (a) MEP plot for $-\text{Cu}-\text{O}-\text{Cu}-\text{O}-\text{Cu}-$ pentamer chain rotation on the $\text{Cu}(100)-c(2 \times 2)$ surface with (b) figures of intermediate and transition states.

row? We choose the pentamer as an example to address this issue. The first rotation step is the same as the first part of the pentamer diffusion along $[010]$, as shown in Figure 9: the top terminal Cu atom in IM8^\wedge moves down one O row to form IM9^+ . The next step is shown in Figures 11a and b: the top Cu atom in IM9^+ continues moving to the right column with a barrier of 0.66 eV. Now the orientation of the pentamer is rotated perpendicular to the vacancy row. The rotation barrier is comparable to the diffusion barriers, and thus the $-\text{Cu}-\text{O}-$ protruding units can change their orientation before connecting into longer chains.

3.4. Cu Ejection near Vacancies. Because surface vacancy formation is a necessary result of $\text{Cu}-\text{O}$ formation, there becomes two types of oxygen adsorption sites: (1) near vacancies and (2) on the perfect $c(2 \times 2)$ surface. To check the sensitivity of the missing-row growth mechanism to the presence of vacancies, we put the second O_2 molecule on the $c(2 \times 2)$ surface next to two Cu vacancies. Figure 12 shows the MEP of the second O_2 dissociation and $-\text{O}-\text{Cu}-\text{O}-$ trimer growth near the vacancies. The DFT+D results indicate that the adsorption energy of O_2 is -0.2 eV, and the overall dissociation barrier is 1.04 eV, a little higher than on the perfect $c(2 \times 2)$ surface. As shown in Figures 12a and b, the subsequent reaction

process is very similar to that on the perfect $c(2 \times 2)$ surface (as shown in Figure 1). The ejection barrier is 1.0 eV, only 0.06 eV higher than that without vacancies. On the basis of these NEB calculations, vacancies on $c(2 \times 2)$ surface do not significantly affect the Cu ejection process.

3.5. Missing-Row Island Formation. According to experiments, it is likely that the ejected Cu atoms diffuse on the surface until they are captured by step defects or trapped at phase boundaries to form monatomic islands.^{9,10,20,47,48} Atomic resolution STM imaging indicates that the topographies of the surface of these ordered islands exhibit the same missing-row structure as the reconstructed substrate, and they always lie in either the $[001]$ or $[010]$ direction. On the basis of the diffusion pathways of Cu and O atoms as described above, we propose a possible path for the missing-row island formation.

Specifically, the trimer, tetramer, and pentamer (at least) are expected to merge into longer $-\text{Cu}-\text{O}-$ chains. The transformation between $-\text{Cu}-\text{O}-$ chains and the missing-row reconstruction requires the incorporation of additional Cu atoms. Although Cu adatoms are highly mobile on the surface, the probability of a single Cu atom existing under the oxidizing conditions is low. Therefore, we speculate that the substrate is an alternative source of Cu atoms. To verify this hypothesis, we

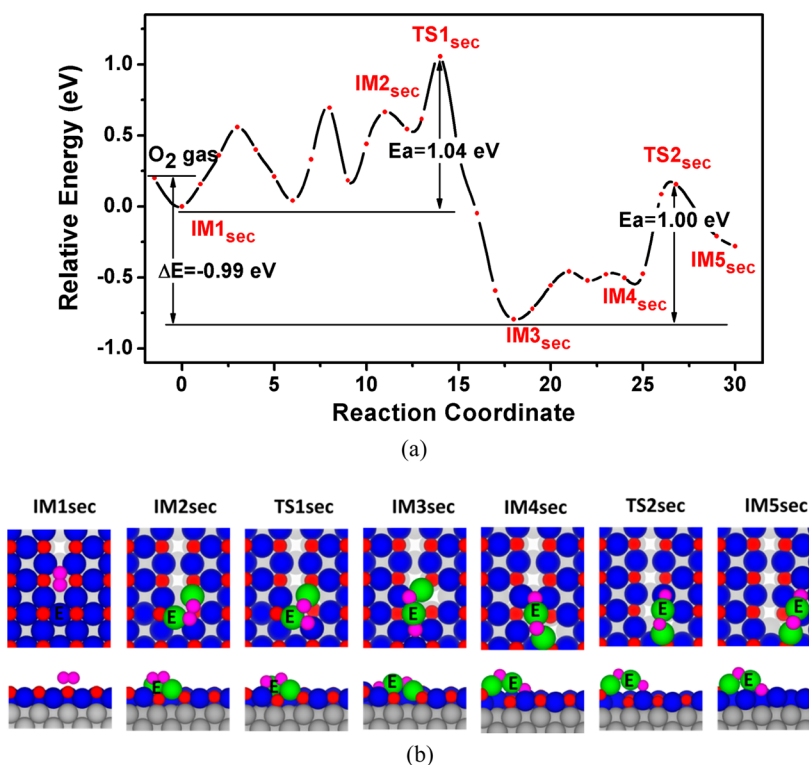


Figure 12. (a) MEP plot for Cu atom ejection from the Cu(100)-c(2 × 2) surface near two vacancies. (b) Upper panels are the top views, and lower panels are the side views of some intermediates and transition states.

start with two $-\text{Cu}-\text{O}-$ chains located on the $c(2 \times 2)$ surface, as illustrated by IS1 in Figure 13b. The MEP of atomic Cu ejection from the substrate is shown in Figure 13a. The barrier for the first Cu atom (labeled as 1) pulled out of the substrate by two $-\text{Cu}-\text{O}-$ chains is 0.64 eV, and the energy of the final state (IS2) is 1.24 eV lower than that of the initial state. The second Cu atom (labeled as 2) is pulled out of the substrate with a similar barrier of 0.67 eV; the system energy further decreases by 1.14 eV. From IS1 to IS3, the energy decreases by 2.38 eV. Thus, missing-row island formation significantly increases the stability of the surface.

Because each subsequent Cu atom can follow the same ejection mechanism, we infer a plausible missing-row island structure, as shown in Figure 14a. As a row of Cu atoms are pulled from the substrate to cross-link the surface $\text{Cu}-\text{O}$ chains, both the top surface layer and subsurface transform into the missing-row patterns at the same time. The picture is clearer when there are more parallel $\text{Cu}-\text{O}$ chains on the surface, as shown in Figure 14a. The [100] and [010] two directions are equivalent on $c(2 \times 2)$, so the missing-row islands can grow along either direction.

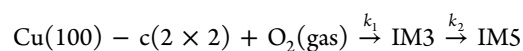
In Figure 14a, the missing rows in the surface and subsurface layer are parallel. The perpendicular structure shown in Figure 14b, however, is energetically more stable. The perpendicular missing-row island can be obtained by rotating pairs of surface Cu atoms contained within the $-\text{Cu}-\text{O}-$ chains 90° to adjacent sites between two O atoms, as shown in Figure 15.

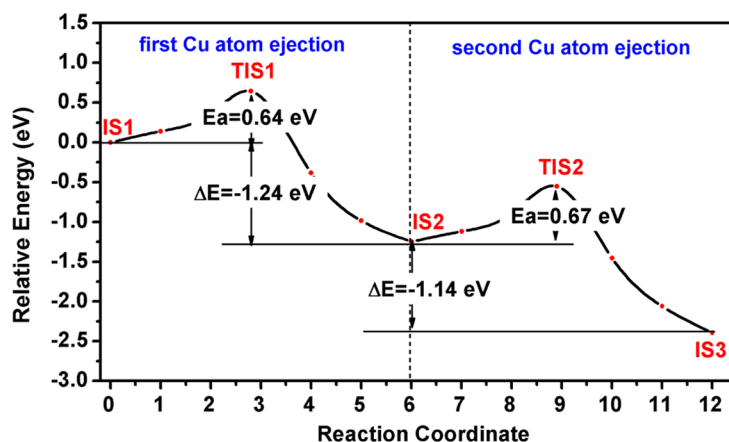
The atoms of the top layer in the IS1_{tran} require small rearrangements to form the IS2_{tran}. This is a barrierless transition, and the energy drops by 0.47 eV. The Cu atom labeled 1 alongside the missing row rotates to its adjacent site between two O atoms. The rotating Cu atom binds to two O atoms to form a $-\text{Cu}-\text{O}-$ chain perpendicular to the original

chain. The barrier for the first Cu rotation is 0.60 eV. The Cu atom labeled 2 rotates in the same way as the first Cu atom, and the barrier is 0.52 eV. Now in IS4_{tran}, one missing row in the top layer is perpendicular to the direction of missing row in the substrate, lowering the energy by 0.74 eV. The Cu atoms labeled 3 and 4 can rotate in the same way to complete the transformation to the perpendicular missing-row island, as shown in Figure 14b. The highest barrier for atom 3 and 4 rotation is 0.64 eV, and the system energy remains the same as IS4_{tran}.

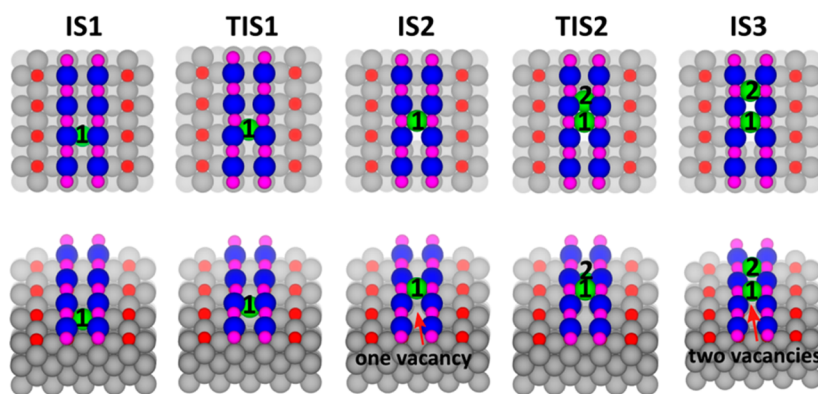
The atomic structure below the top layer of the missing-row islands are not known experimentally due to a lack of characterization tools with sufficient ability to resolve the multilayer atomic structures in small domains. Our simulations, however, provide a clear prediction about the island structure, both in the surface and subsurface.

3.6. Facilitating Experimental Verification. Molecular O_2 dissociation is a critical step in our proposed oxidation mechanism. As shown in Figure 10, there is a substantial energy drop from IM2 to IM3, and the stability of IM3 requires a barrier of 0.96 eV to form IM5. To help make connection with experiments, we simulated a STM image of the IM3 structure shown in Figure 16a. In the simulated STM image, the brightest features are associated with raised $-\text{O}-\text{Cu}-\text{O}-$ trimers which look like dumbbells. The remaining small gray spots are the $-\text{Cu}-\text{O}-$ chains in the Cu(100)- $c(2 \times 2)$ surface. The concentration of IM3 structures on the surface during the time scale of oxidation is an important factor for determining the possibility of IM3 being observed in experiments. Consider the following reaction:



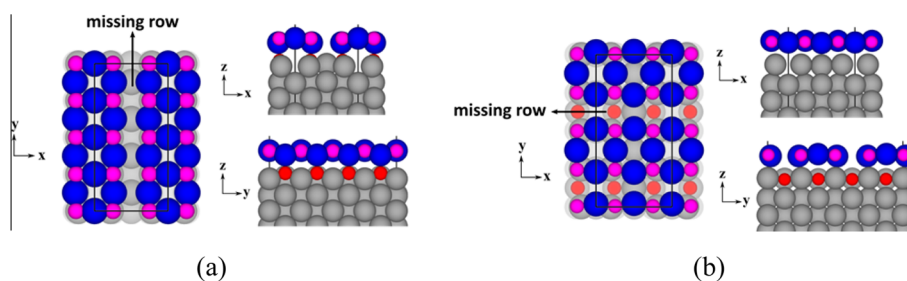


(a)



(b)

Figure 13. (a) MEP for Cu atom ejection from the Cu(100)- $c(2 \times 2)$ surface to form parallel missing-row islands. (b) Upper panels are top views, and lower panels are the side views of the intermediate and transition states. For illustration purposes, the substrate Cu and O atoms are depicted by gray and red spheres; Cu and O atoms in the add-chains are blue and magenta, respectively, and the ejected Cu atoms are shown as green spheres.



(a)

(b)

Figure 14. (a) Top and side views of (a) the parallel and (b) the perpendicular missing-row island. Top-layer Cu and O atoms are depicted as blue and magenta spheres; the substrate Cu and O atoms are gray and red, respectively.

The values of k_1 and k_2 are estimated from eq 1 with corresponding barriers of 0.95 and 0.96 eV, respectively (see Figure 10). The first reverse reaction is neglected because the barrier is higher than 1.5 eV. In an additional approximation, IM5 is set to an absorbing state because the process from IM5 to long Cu–O chains is relatively fast and highly exothermic. IM3 coverage vs time are calculated by solving the rate equations analytically and are plotted in Figure 16b. We chose five different temperatures within the experimental range of oxidation experiments. The IM3 coverage clearly increases initially and decreases slowly toward equilibrium. It should be possible to detect the IM3 structure at low temperature (≤ 350

K) due to a persistent high coverage over a time scale of seconds to minutes.

4. CONCLUSION

DFT calculations were employed to investigate the kinetics and energetics of phase transition during the early stages of Cu(100) oxidation. We propose a novel mechanism for Cu atom ejection from the Cu(100)- $c(2 \times 2)$ surface involving adsorbed O_2 molecules. Once O_2 dissociates, O atoms promote the ejection of Cu atoms from the substrate with a barrier of 0.96 eV. We find diffusion mechanisms by which the Cu and O atoms diffuse away from the vacancies onto the defect-free $c(2 \times 2)$ surface. Three Cu–O chain species, the $-O-Cu-O-$

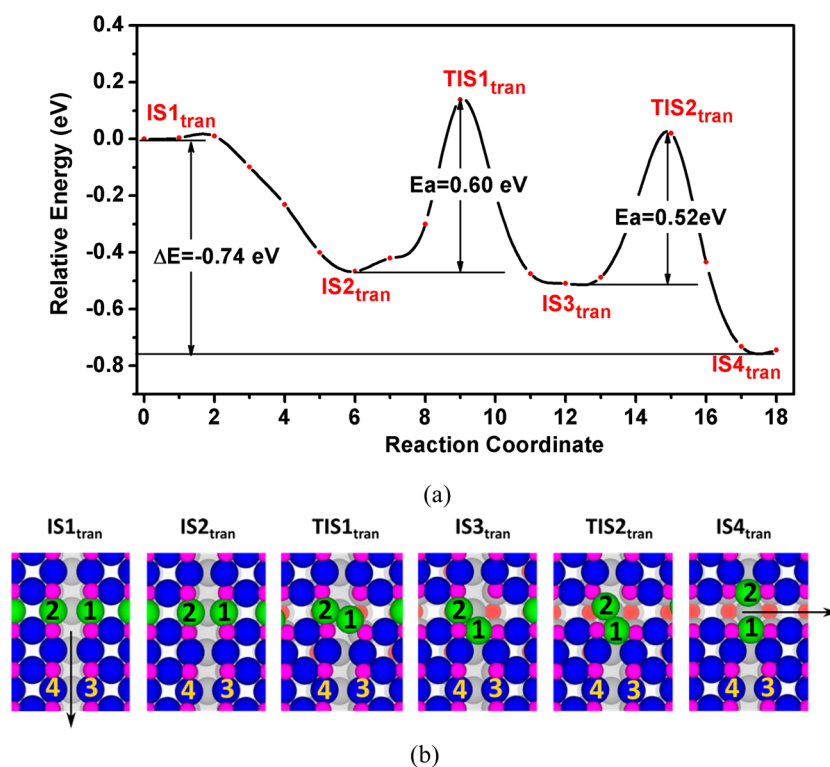


Figure 15. (a) MEP plot for Cu atom transition from a parallel missing-row island to form a perpendicular missing-row island and (b) structures of intermediate configurations. The top-layer Cu and O atoms are depicted as blue and magenta spheres, and the substrate Cu and O atoms are gray and red, respectively; the rotating Cu atoms are green. The arrow indicates the direction of the missing row in the top layer.

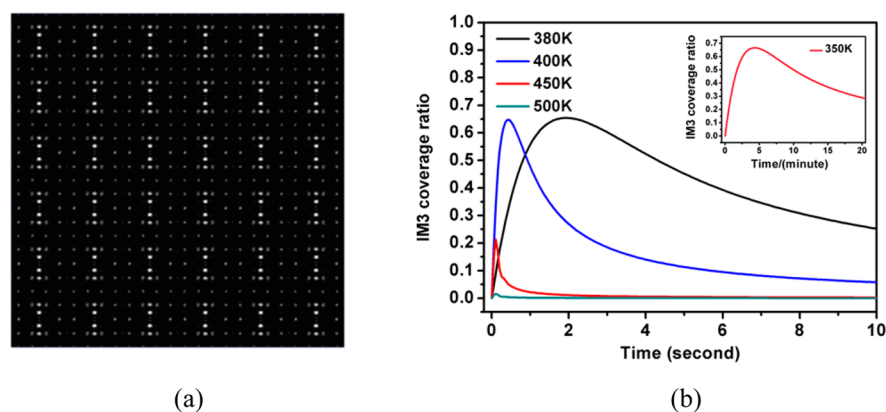


Figure 16. (a) Simulated STM image for the IM3 structure. (b) IM3 coverage ratio vs time at different temperatures.

trimer, $-\text{Cu}-\text{O}-\text{Cu}-\text{O}-$ tetramer, and $-\text{Cu}-\text{O}-\text{Cu}-\text{O}-\text{Cu}-$ pentamer, are found to form and rapidly diffuse on the surface. The concerted mechanisms which facilitate this diffusion involve sequential motion of the chain ends to maintain Cu–O bonding as much as possible. The Cu–O units can also rotate perpendicular to the missing row that is created upon their formation. Neighboring $-\text{Cu}-\text{O}-$ chains can pull Cu atoms from the substrates to form two MRR layers with a barrier of 0.67 eV. The energy decreases with each Cu atom ejection from the substrate to form these missing-row islands. Moreover, we find the perpendicular missing-row island is more stable than the parallel missing-row island, and the barrier of this transition is 0.60 eV. Finally, we suggest possible experiments to verify the mechanisms of missing-row formation proposed in this work.

■ ASSOCIATED CONTENT

📄 Supporting Information

The Supporting Information is available free of charge on the ACS Publications website at DOI: [10.1021/acs.chemmater.6b02722](https://doi.org/10.1021/acs.chemmater.6b02722).

Additional figures of intermediate and transition states (PDF)

■ AUTHOR INFORMATION

Corresponding Authors

*E-mail: henkelman@utexas.edu.

*E-mail: lrl@cqu.edu.cn.

ORCID

Graeme Henkelman: [0000-0002-0336-7153](https://orcid.org/0000-0002-0336-7153)

Author Contributions

[§]X.L. and P.X. contributed equally.

Notes

The authors declare no competing financial interest.

ACKNOWLEDGMENTS

We gratefully acknowledge the National Science Foundation (Grant DMR-1410335), the Welch Foundation (Grant F-1841), and the Texas Advanced Computing Center. X.L. thanks the China Scholarship Council for financial support.

REFERENCES

- (1) Huang, T.; Tsai, D. CO oxidation behavior of copper and copper oxides. *Catal. Lett.* **2003**, *87*, 173–178.
- (2) Jing, F.; Zhang, Y.; Luo, S.; Chu, W.; Zhang, H.; Shi, X. Catalytic synthesis of 2-methylpyrazine over Cr-promoted copper based catalyst via a cyclo-dehydrogenation reaction route. *J. Chem. Sci.* **2010**, *122*, 621–630.
- (3) Over, H.; Kim, Y. D.; Seitsonen, A. P.; Wendt, S.; Lundgren, E.; Schmid, M.; Varga, P.; Morgante, A.; Ertl, G. Atomic-scale structure and catalytic reactivity of the RuO₂(2)(110) surface. *Science* **2000**, *287*, 1474–1476.
- (4) Lara-Castells, M. P.; Krause, J. L. Theoretical study of the interaction of molecular oxygen with a reduced TiO₂ surface. *Chem. Phys. Lett.* **2002**, *354*, 483–490.
- (5) Wendt, S.; Schaub, R.; Matthiesen, J.; Vestergaard, E. K.; Wahlström, E.; Rasmussen, M. D.; Thosttrup, P.; Molina, L. M.; Lagsgaard, E.; Stensgaard, I.; Hammer, B.; Besenbacher, F. Oxygen vacancies on TiO₂(110) and their interaction with H₂O and O₂: A combined high-resolution STM and DFT study. *Surf. Sci.* **2005**, *598*, 226–245.
- (6) Le, D.; Stolbov, S.; Rahman, T. S. Reactivity of the Cu₂O(100) surface: Insights from first principles calculations. *Surf. Sci.* **2009**, *603*, 1637–1645.
- (7) Zhang, R. G.; Liu, H. Y.; Zheng, H. Y.; Ling, L. X.; Li, Z.; Wang, B. J. Adsorption and dissociation of O₂ on the Cu₂O(1 1 1) surface: Thermochemistry, reaction barrier. *Appl. Surf. Sci.* **2011**, *257*, 4787–4794.
- (8) Westerstrom, R.; Gustafson, J.; Resta, A.; Mikkelsen, A.; Andersen, J. N.; Lundgren, E.; Seriani, N.; Mittendorfer, F.; Schmid, M.; Kiklovits, J.; Varga, P.; Ackermann, M. D.; Frenken, J. W. M.; Kasper, N. A. Stierle. Oxidation of Pd (553): From ultrahigh vacuum to atmospheric pressure. *Phys. Rev. B: Condens. Matter Mater. Phys.* **2007**, *76*, 155410–155419.
- (9) Lampimäki, M.; Lahtonen, K.; Hirsimäki, M.; Valden, M. Nanoscale oxidation of Cu(100): Oxide morphology and surface reactivity. *J. Chem. Phys.* **2007**, *126*, 1–7.
- (10) Lahtonen, K.; Hirsimäki, M.; Lampimäki, M.; Valden, M. Oxygen adsorption-induced nanostructures and island formation on Cu(100): Bridging the gap between the formation of surface confined oxygen chemisorption layer and oxide formation. *J. Chem. Phys.* **2008**, *129*, 1–9.
- (11) Zeng, H. C.; McFarlane, R. A.; Mitchell, K. A. R. A LEED crystallographic investigation of some missing-row models for the Cu(100)-(2√2 × √2)R45°-O surface structure. *Surf. Sci.* **1989**, *208*, L7–L14.
- (12) Yokoyama, T.; Arvanitis, D.; Lederer, T.; Tischer, M.; Tröger, L.; Baberschke, K.; Comelli, G. Adsorption of oxygen on Cu(100). II. Molecular adsorption and dissociation by means of O K-edge x-ray-absorption fine structure. *Phys. Rev. B: Condens. Matter Mater. Phys.* **1993**, *48*, 15405–15416.
- (13) Puisto, A.; Pitkanen, H.; Alatalo, M.; Jaatinen, S.; Salo, P.; Foster, A. S.; Kangas, T.; Laasonen, K. Adsorption of atomic and molecular oxygen on Cu(100). *Catal. Today* **2005**, *100*, 403–406.
- (14) Alatalo, M.; Jaatinen, S.; Salo, P.; Laasonen, K. Oxygen adsorption on Cu(100): First-principles pseudopotential calculations. *Phys. Rev. B: Condens. Matter Mater. Phys.* **2004**, *70*, 3600–3606.
- (15) Jaatinen, S.; Blomqvist, J.; Salo, P.; Puisto, A.; Alatalo, M.; Hirsimäki, M.; Ahonen, M.; Valden, M. Adsorption and diffusion dynamics of atomic and molecular oxygen on reconstructed Cu(100). *Phys. Rev. B: Condens. Matter Mater. Phys.* **2007**, *75*, 1–8.
- (16) Jensen, F.; Besenbacher, F.; Laegsgaard, E.; Stensgaard, I. Dynamics of oxygen-induced reconstruction of Cu(100) studied by scanning tunneling microscopy. *Phys. Rev. B: Condens. Matter Mater. Phys.* **1990**, *42*, 9206–9209.
- (17) Wöll, C.; Wilson, R. J.; Chiang, S.; Zeng, H. C.; Mitchell, K. A. R. Oxygen on Cu(100) surface structure studied by scanning tunneling microscopy and by low-energy-electron-diffraction multiple-scattering calculations. *Phys. Rev. B: Condens. Matter Mater. Phys.* **1990**, *42*, 11926–11929.
- (18) Iddir, H.; Fong, D. D.; Zapol, P.; Fuoss, P. H.; Curtiss, L. A.; Zhou, G. W.; Eastman, J. A. Order-disorder phase transition of the Cu(001) surface under equilibrium oxygen pressure. *Phys. Rev. B: Condens. Matter Mater. Phys.* **2007**, *76*, 1–4.
- (19) Fujita, T.; Okawa, Y.; Matsumoto, Y.; Tanaka, K. Phase boundaries of nanometer scale c(2 × 2)-O domains on the Cu(100) surface. *Phys. Rev. B: Condens. Matter Mater. Phys.* **1996**, *54*, 2167–2174.
- (20) Tanaka, K.; Fujita, T.; Okawa, Y. Oxygen induced order-disorder restructuring of a Cu(100) surface. *Surf. Sci.* **1998**, *401*, L407–L412.
- (21) Bonini, N.; Kokalj, A.; Dal Corso, A.; de Gironcoli, S.; Baroni, S. Structure and dynamics of the missing-row reconstruction on O/Cu(001) and O/Ag(001). *Surf. Sci.* **2006**, *600*, 5074–5079.
- (22) Harrison, M. J.; Woodruff, D. P.; Robinson, J.; Sander, D.; Pan, W.; Kirschner, J. Adsorbate-induced surface reconstruction and surface-stress changes in Cu(100)/O: Experiment and theory. *Phys. Rev. B: Condens. Matter Mater. Phys.* **2006**, *74*, 1–7.
- (23) Kittel, M.; Polcik, M.; Terborg, R.; Hoeft, J. T.; Baumgartel, P.; Bradshaw, A. M.; Toomes, R. L.; Kang, J. H.; Woodruff, D. P.; Pascal, M.; Lamont, C. L. A.; Rotenberg, E. The structure of oxygen on Cu(100) at low and high coverages. *Surf. Sci.* **2001**, *470*, 311–324.
- (24) Duan, X.; Warschkow, O.; Soon, A.; Delley, B.; Stampfl, C. Density functional study of oxygen on Cu(100) and Cu(110) surfaces. *Phys. Rev. B: Condens. Matter Mater. Phys.* **2010**, *81*, 1–15.
- (25) Jacobsen, K. W.; Norskov, J. K. Theory of the oxygen-induced restructuring of Cu(110) and Cu(100) surfaces. *Phys. Rev. Lett.* **1990**, *65*, 1788–1791.
- (26) Stolbov, S.; Rahman, T. S. Role of Long Range Interaction in Oxygen Superstructure Formation on Cu(001) and Ni(001). *Phys. Rev. Lett.* **2002**, *89*, 116101.
- (27) Sekiba, D.; Inokuchi, T.; Wakimoto, Y.; Yagi-Watanabe, K.; Fukutani, H. Electronic structure of Cu(100) (2√2 × √2)R45°-O surface: angle-resolved photoemission spectroscopy and tight-binding calculation. *Surf. Sci.* **2000**, *470*, 43–52.
- (28) Lee, M. Y.; McGaughey, A. J. H. Energetics and kinetics of the c(2 × 2) to (2√2 × √2)R45° transition during the early stages of Cu(100) oxidation. *Phys. Rev. B: Condens. Matter Mater. Phys.* **2011**, *83*, 1–8.
- (29) Kangas, T.; Laasonen, K. Formation of a missing-row reconstruction on a Cu(100) surface: an atom scale density functional theory based study. *Surf. Sci.* **2012**, *606*, 192–201.
- (30) Yang, J. C.; Yeadon, M.; Kolasa, B.; Gibson, J. M. Surface reconstruction and oxide nucleation due to oxygen interaction with Cu(001) observed by in situ ultra-high vacuum transmission electron. *Microsc. Microanal.* **1998**, *4*, 334–339.
- (31) Zhou, G. W.; Yang, J. C. Temperature effect on the Cu₂O oxide morphology created by oxidation of Cu(001) as investigated by in situ UHV-TEM. *Appl. Surf. Sci.* **2003**, *210*, 165–170.
- (32) Zhou, G. W.; Yang, J. C. Formation of Quasi-One-Dimensional Cu₂O structures by in situ oxidation of Cu(100). *Phys. Rev. Lett.* **2002**, *89*, 106101.
- (33) Zhou, G. W.; Yang, J. C. Initial oxidation kinetics of Cu(100), (110), and (111) thin films investigated by in situ ultra-high-vacuum transmission electron microscopy. *J. Mater. Res.* **2005**, *20*, 1684–1694.

- (34) Lee, M.; McGaughey, A. J. H. Energetics of oxygen embedment into unreconstructed and reconstructed Cu(100) surfaces: Density functional theory calculations. *Surf. Sci.* **2009**, *603*, 3404–3409.
- (35) Lee, M.; McGaughey, A. J. H. Role of sub-surface oxygen in Cu(100) oxidation. *Surf. Sci.* **2010**, *604*, 1425–1431.
- (36) Kangas, T.; Laasonen, K. DFT study of reconstructed Cu(100) surface with high oxygen coverages. *Surf. Sci.* **2008**, *602*, 3239–3245.
- (37) Kresse, G.; Hafner, J. Ab initio molecular dynamics for liquid metals. *Phys. Rev. B: Condens. Matter Mater. Phys.* **1993**, *47*, 558–561.
- (38) Kresse, G.; Hafner, J. Ab Initio Molecular-Dynamics simulation of the liquid-metal–amorphous-semiconductor transition in germanium. *Phys. Rev. B: Condens. Matter Mater. Phys.* **1994**, *49*, 14251–14269.
- (39) Kresse, G.; Furthmüller, J. Efficiency of ab-initio total energy calculations for metals and semiconductors using a plane-wave basis set. *Comput. Mater. Sci.* **1996**, *6*, 15–50.
- (40) Kresse, G.; Furthmüller, J. Efficient iterative schemes for ab initio total-energy calculations using a plane-wave basis set. *Phys. Rev. B: Condens. Matter Mater. Phys.* **1996**, *54*, 11169–11186.
- (41) Perdew, J. P.; Burke, K.; Ernzerhof, M. Generalized gradient approximation made simple. *Phys. Rev. Lett.* **1996**, *77*, 3865–3868.
- (42) Blöchl, P. E. Projector augmented-wave method. *Phys. Rev. B: Condens. Matter Mater. Phys.* **1994**, *50*, 17953–17979.
- (43) Kresse, G.; Joubert, D. From ultrasoft pseudopotentials to the projector augmented-wave method. *Phys. Rev. B: Condens. Matter Mater. Phys.* **1999**, *59*, 1758–1775.
- (44) Monkhorst, H. J.; Pack, J. D. Special Points for Brillouin-Zone Integrations. *Phys. Rev. B* **1976**, *13*, 5188–5192.
- (45) Grimme, S.; Antony, J.; Ehrlich, S.; Krieg, H. A Consistent and Accurate ab initio Parametrization of Density Functional Dispersion Correction (DFT-D) for the 94 Elements H–Pu. *J. Chem. Phys.* **2010**, *132*, 1–19.
- (46) Henkelman, G.; Uberuaga, B. P.; Jonsson, H. A climbing image nudged elastic band method for finding saddle points and minimum energy paths. *J. Chem. Phys.* **2000**, *113*, 9901–9904.
- (47) Tanaka, K.; Matsumoto, Y.; Fujita, T.; Okawa, Y. Nano-scale patterning of metal surfaces by adsorption and reaction. *Appl. Surf. Sci.* **1998**, *130*, 475–483.
- (48) Fujita, T.; Okawa, Y.; Tanaka, K. STM study of preferential growth of one-dimensional nickel islands on a Cu(100) ($2\sqrt{2} \times \sqrt{2}$) $R45^\circ$ -O surface. *Appl. Surf. Sci.* **1998**, *130*, 491–496.